Research Square

Preprints are preliminary reports that have not undergone peer review.
They should not be considered conclusive, used to inform clinical practice,
or referenced by the media as validated information.

Response-Specific Effects of Strontium and Copper–Tin Modification on Cutting Force and Surface Roughness in the Dry Turning of an Al-12Si Casting Alloy

Mustafa Keser

mustafakeser@zoho.com

Independent Researcher

Research Article

Keywords: Al-12Si, Modification, Strontium, Machinability, Surface roughness

Posted Date: November 4th, 2026

DOI: https://doi.org/10.21203/rs.3.rs-10685150/v1

License: This work is licensed under a Creative Commons Attribution 4.0 International License.
Read Full License

Additional Declarations: No competing interests reported.

Response-Specific Effects of Strontium and Copper–Tin Modification on Cutting Force and Surface Roughness in the Dry Turning of an Al-12Si Casting Alloy

Mustafa Keser[1]

[1] Independent Researcher, Sakarya, Turkey
ORCID: 0000-0002-0534-5417

Corresponding author: Mustafa Keser · mustafakeser@zoho.com

Abstract

Purpose Modification of Al-12Si casting alloys is usually treated as a single intervention, and cutting force and surface roughness are usually assumed to move together. This study asks whether the two additions used in modification act on the same machinability criteria, and whether the two criteria share a mechanism.

Methods A 36-run full-factorial dataset from the dry turning of Etial 140 (Al-12Si) modified with Al10Sr, CuSn5 and Al10Sr+CuSn5 master alloys was analysed. The four groups form an embedded 2 × 2 design with respect to strontium (0.155 wt%) and copper–tin (1.05 wt% Cu), allowing the modification effect to be decomposed into orthogonal components. All inference is conducted at the experimental-run level. Bootstrap confidence intervals were used to bound null effects, and the contribution of built-up edge was assessed by conditional-association analysis using ordinal scoring of insert SEM images.

Results The effects are response-specific. Strontium raises the cutting force by 44 % ($F(1,16) = 26.38$; $p < 0.001$) with no detectable change in surface roughness ($p = 0.65$); the CuSn5 addition degrades surface roughness by 71 % ($F(1,16) = 182.52$; $p < 0.001$) with no detectable change in cutting force ($p = 0.94$). Both null effects are bounded below half the magnitude of the opposing effect. Including built-up edge attenuates the CuSn5 effect on roughness by only 11 %. Microscopy shows discrete angular second-phase particles in the CuSn5-bearing groups alone; their identity was not established.

Conclusion Machinability cannot be summarised by a single criterion: cutting force and surface roughness respond to different additions, so alloy selection must follow from which criterion takes priority.

Keywords Al-12Si · Modification · Strontium · Machinability · Surface roughness

---

1 Introduction

Al-Si casting alloys are widely used in automotive and aerospace components because they combine low density, good castability and adequate mechanical strength [1]. In near-eutectic Al-12Si alloys the acicular, plate-like morphology of the eutectic silicon limits both ductility and machinability.

1.1 Modification and microstructure

The principal remedy is **modification**. Trace additions of strontium, sodium or antimony alter the nucleation and growth dynamics of the eutectic silicon, converting the coarse plate morphology into a fine fibrous structure [2, 3]. The scale of the effect is remarkable: strontium can transform the eutectic structure at additions of the order of 0.01–0.02 wt% [2, 4]. Modification with rare-earth elements produces a comparable morphological transformation [5]. The identity of the modifying element affects the eutectic formation temperature and nucleation density in different ways [6, 7], and interactive behaviour arises when bismuth and antimony are present together with strontium [8].

Copper and tin are added for a different purpose. Copper can increase strength and hardness through Cu-rich precipitates and intermetallic phases, depending on alloy composition and thermal history; tin improves wear resistance and bearing properties [9]. The microstructural consequence of copper, however, is not a refinement of the eutectic silicon but the formation of a **separate family of hard, brittle intermetallic phases**, principally Al_2Cu, in the interdendritic regions [8, 9]. The additions collected under the heading “modification” therefore make two qualitatively different interventions in the microstructure.

1.2 Machinability of Al-Si alloys

Both interventions can be traced separately in the machinability literature. The effect of silicon content is comparatively well documented: comparisons of AlSi6, AlSi12 and AlSi18 alloys show that increasing silicon raises both cutting force and tool wear [10, 11], and silicon particle size has been linked directly to tool wear [12]. The decisive role of the tool–workpiece pair has also been emphasised; studies comparing coated and uncoated carbide inserts on Al-12 % Si report that the coating alters adhesion behaviour [13, 14].

The effect of modifying elements on machinability has received less attention. Barzani and co-workers examined the influence of bismuth, antimony and strontium on the microstructure, thermal behaviour and machinability of Al-Si and Al-Si-Cu alloys [15, 16]. Among studies of copper-bearing alloys, the comparison of Al-7Si, Al-7Si-4Zn and Al-7Si-4Zn-3Cu by Bayraktar and Afyon [17] is one of the few that addresses the effect of a copper addition on machinability criteria directly. Predictive models for the surface roughness of Al-Si-Cu-Fe die-casting alloys containing different additives have also been reported [18].

The study closest to the present one is that of Basavakumar and co-workers, who turned **Al-12Si and Al-12Si-3Cu** alloys and compared cutting force and surface integrity [19]. The same alloy pair, the same machining operation and the same two responses were

examined. The present work differs in that the copper and strontium effects are **statistically separated within a single dataset**.

The relationship between machined surface quality and microstructure has also been investigated. Grum and Kisin showed in a two-part study that workpiece microstructure influences both cutting forces and surface integrity in turning [20, 21]. In aluminium-based systems containing hard second-phase particles — of which particle-reinforced composites are the extreme case — the particles are reported to accelerate tool wear and degrade surface quality [22, 23, 24].

A recurrent phenomenon in machining aluminium is **built-up edge (BUE) formation**. The classic study of Bao and Stevenson established that aluminium adheres to the tool face, forming a mass on the cutting edge that builds up and breaks away periodically [25]. Because the detachment of this mass damages the machined surface, material-dependent differences in surface quality are frequently attributed to built-up edge. It should be noted, however, that a drilling study reported the copper-bearing 319 alloy to give more than twice the tool life of the Al-Si-Mg-based 356 alloy, with edge build-up *decreasing* as hardness rose [26] — an expectation that copper *increases* built-up edge is therefore not established in the literature.

1.3 Two limitations and the aim of this study

Despite this body of work, most studies of modification and machinability remain descriptive: cutting force and surface roughness are reported by parameter level, without decomposing the relative contributions of the factors. This approach has two limitations.

First, "modification" is treated as a single operation. As summarised in Sect. 1.1, strontium refines the eutectic silicon whereas copper–tin introduces a separate family of intermetallic phases in the interdendritic regions. There is no reason why these two changes should affect machinability in the same way; yet when alloys are grouped into a single "modified" category, the distinction cannot be measured.

Second, cutting force and surface roughness are usually treated together, with a direct causal link assumed between them: higher force implies more vibration and deformation, hence a poorer surface. This assumption does not hold universally and requires **testing**, particularly where material composition varies.

Operational definition. Throughout this paper machinability is evaluated specifically through two responses — cutting force (Fc) and arithmetic mean surface roughness (Ra) — with built-up edge and chip morphology treated as secondary explanatory observations. Tool life and tool wear were not measured and no claim is made about them.

The aim of this study is to exploit the embedded 2 × 2 structure formed by the four material groups in order to **decompose the modification effect into strontium and copper–tin components**, and to test whether the two machinability criteria — cutting force and surface roughness — respond to the same underlying mechanism.

2 Materials and Methods

2.1 Data provenance and scope

The experimental dataset analysed here was obtained in the author's master's thesis work [27]. The design, execution and measurement of the experiments belong to that work; **the contribution of the present paper is the statistical analysis.** To make the boundary explicit:

	Already reported in [27]	New in this paper
Data	36 runs: Fc, Ff, Ra (3 readings), hardness, chemical analysis	—
Micrographs	Optical microstructures (Fig. 1)	—
Insert SEM images	Images themselves	Ordinal built-up-edge scoring by the author, with an AI-assisted preliminary set for comparison
Chip photographs	Photographs themselves	—
Analysis	Descriptive comparison by parameter level	Analysis of variance with Sr/CuSn5 decomposition; bootstrap confidence intervals on null effects; multiple-comparison correction; sensitivity analysis over data variants; conditional-association analysis for built-up edge; Taguchi S/N; cross-validated model comparison; flexible-learner comparison

Figure 1 and the chip photographs are reproduced from the source work and are identified as such in their captions; Figs. 2–7 are generated here from the raw data. No statistical test reported in this paper appears in [27]. The thesis is publicly available through the Turkish Council of Higher Education Thesis Centre under the number given in the reference list, so the extent of the overlap can be verified directly.

2.2 Materials and the embedded 2 × 2 design

Etial 140 (Al-~12Si) casting alloy was used as the base material. Four material groups were examined, comprising the unmodified base alloy and three modified variants (Table 1).

Table 1 Composition and hardness of the experimental materials

Group	Master alloy	Si (%)	Sr (%)	Cu (%)	Sn (%)	Hardness (HB)
A	— (unmodified)	~12	—	—	—	85.7
B	CuSn5	~12	—	1.054	0.067	90.4
C	Al10Sr	~12	0.156	—	—	86.2
D	Al10Sr + CuSn5	~12	0.153	1.054	0.074	99.2

Source: [27]

The notable feature of Table 1 is that the four groups constitute an **embedded 2 × 2 factorial design**. In the strontium-bearing groups (C and D) the Sr content is practically identical (0.156 and 0.153 %); in the copper–tin-bearing groups (B and D) the Cu content is identical (1.054 %) and the Sn contents are close (0.067 and 0.074 %). This permits the three degrees of freedom of the material factor to be decomposed into three orthogonal components:

- **Sr effect** (1 df): C + D versus A + B
- **CuSn5 effect** (1 df): B + D versus A + C
- **Sr × CuSn5 interaction** (1 df): departure of the joint behaviour from additivity

This decomposition was not intended in the original experimental design, but it is valid because the compositions are balanced, and it forms the basis of the analysis strategy adopted here.

The material side of the decomposition is confirmed by microscopy (Fig. 1). In the unmodified group A the eutectic silicon forms a long, coarse, acicular network. In the strontium-bearing groups C and D this structure has been converted into a **fine fibrous matrix** that cannot be resolved individually at 200× magnification; that is, **strontium modification took place as intended.** In the copper–tin-bearing groups B and D, by contrast, **discrete, angular, dark second-phase particles** are visible that are absent in A and C. In group B the eutectic silicon has additionally shortened and become blocky — a change different in kind from the fibrous refinement produced by strontium.

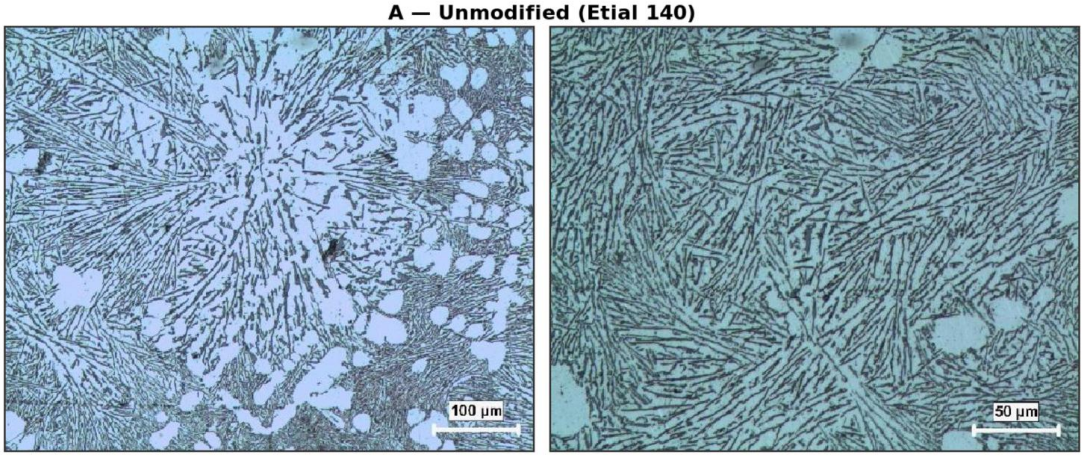
In short, the two additions make **qualitatively different** interventions in the microstructure: strontium refines the eutectic and renders it continuous, whereas copper–tin introduces discrete hard particles. This observation is the basis of the mechanism discussed in Sect. 4.2.

> **Fig. 1** Microstructures of the four material groups at 100× and 200× optical magnification. **A** unmodified — long, coarse, acicular eutectic Si network. **B** CuSn5 — shortened and blocky Si, together with discrete angular dark particles. **C** Al10Sr — fine fibrous, unresolved eutectic matrix; successful modification. **D**

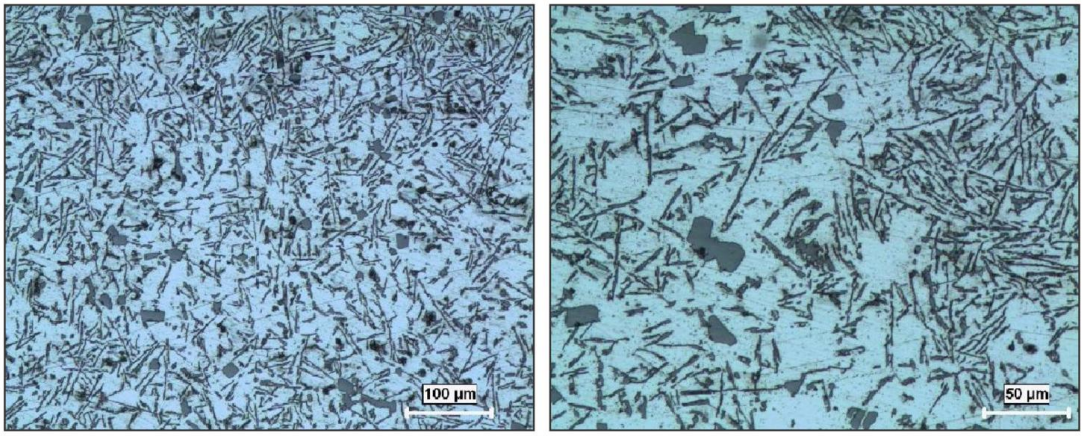
Al10Sr+CuSn5 — modified matrix with discrete angular particles. Scale bars: 100 μm (left column), 50 μm (right column)

100× 200×

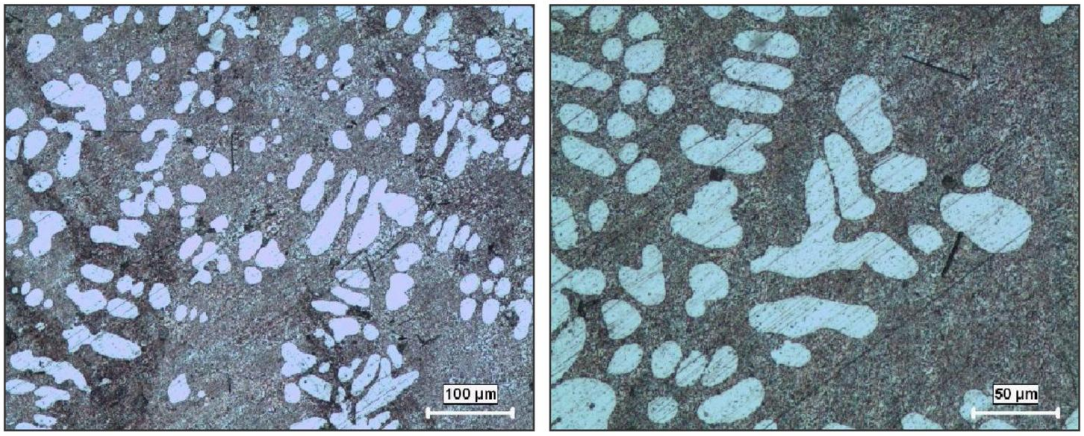
A — Unmodified (Etial 140)



B — Etial 140 + CuSn5



C — Etial 140 + Al10Sr



D — Etial 140 + Al10Sr + CuSn5

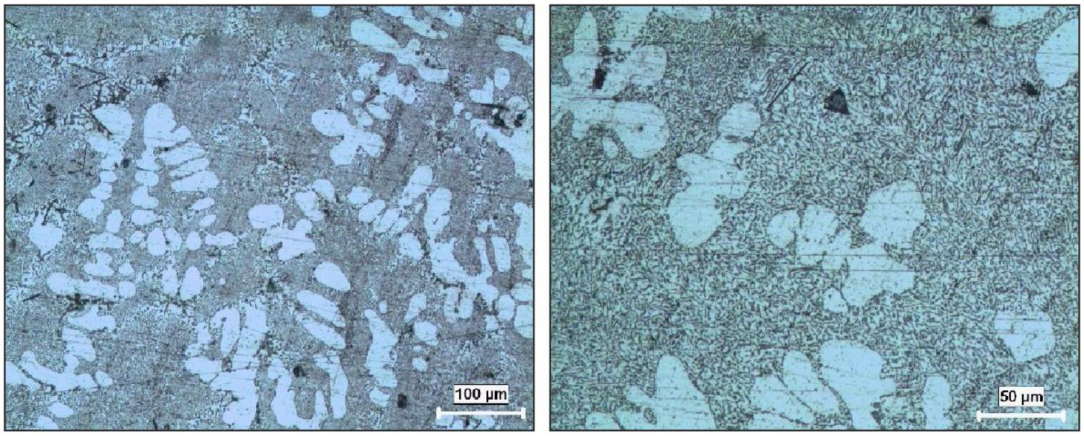


Fig. 1

At optical magnification the **phase of these particles cannot be identified.** The composition and the literature (Sect. 4.2) point to Al_2Cu-type copper intermetallics; however, in an etched Al-Si section the dark phases are predominantly silicon, and a definitive distinction requires energy-dispersive X-ray spectroscopy (EDS) or backscattered-electron imaging. Neither was performed in this study. The term **"discrete hard second phase"** is therefore used below, and no claim is made as to phase identity.

2.3 Machining experiments and measurement

Specimens cut from Ø20 mm bars were faced to a length of 50 mm, centre-drilled at both ends, and the experiments were performed by **longitudinal turning between centres**. A conventional TOS lathe (spindle power 5.5 kW; 22–2000 rpm) was used under **dry cutting conditions**.

The cutting tool was a titanium diboride PVD-coated cemented carbide insert of Kennametal grade KC5410 (ISO catalogue no. TCGT110204HP; nose radius Rε = 0.4 mm). The tool holder was selected in accordance with ISO 3685 [28].

After each experiment the insert was imaged in a scanning electron microscope. All images were acquired at **100× magnification, 20 kV accelerating voltage and a 2.30 mm field of view**, with a constant pixel size of 2.244 µm. The majority were recorded with the **secondary-electron (SE) detector**; in three experiments a backscattered-electron (BSE) detector was used, and because BSE provides compositional rather than topographic contrast these three images are not suitable for topographic comparison (Sect. 5). Although magnification and field of view were constant, **the tilt and orientation of the insert varied between images, so the deposit area was not measured in pixels**; the ordinal scale defined in Sect. 4.1 was used instead. The grades used in the analysis are the author's; a preliminary set produced with AI assistance (Sect. 2.5) is reported alongside them as a consistency check (Sect. 4.1).

Chip samples were collected after each experiment and photographed alongside a scaled rule.

The cutting parameters were arranged as a full factorial:

- **Cutting speed (V):** 35 · 95 · 135 m/min
- **Feed (f):** 0.08 · 0.16 · 0.32 mm/rev
- **Depth of cut (a):** 1 mm (constant)

4 materials × 3 cutting speeds × 3 feeds = **36 experiments**, one run per cell.

Cutting force (Fc) and feed force (Ff) were measured simultaneously with a two-component dynamometer mounted on the lathe, the values recorded over the cutting period being averaged. Surface roughness was measured with a Mahr Perthometer M1 portable instrument in accordance with ISO 4288 [29] (sampling length λ = 0.25 mm; evaluation length L = 1.75 mm; Gaussian filter). **Three measurements** were taken from each machined region, and their arithmetic mean (Ra) was used in the analyses. These

three readings are **repeated measurements on the same machining run**, not independently machined specimens; they are therefore treated as measurement replicates throughout and are used only to characterise measurement precision (Sect. 2.4).

2.4 Statistical analysis

The analyses of variance were constructed with the material factor decomposed into the strontium and copper–tin components defined in Sect. 2.2, including main effects and all two-factor interactions. Because the design is balanced, the components are orthogonal and the sums of squares are additive.

Both responses are analysed at the experimental-run level (n = 36). For cutting force there is a single observation per cell. For surface roughness the three readings per run are averaged to a single run value before analysis, because they are measurement replicates rather than independent experimental replicates; treating them as the latter would inflate the error degrees of freedom and overstate the precision of the F tests. In both cases the error term is therefore estimated by **pooling the highest-order interaction terms** (df = 16). This is a common approach in unreplicated factorial designs, but it rests on an assumption that should be stated: the pooled terms are taken to contain no systematic effect. The assumption is supported here by those terms being small and non-significant relative to the retained effects, but it is an assumption and not a measured pure error. The three roughness readings are used only to characterise measurement precision (Sect. 3.2); the inferential error term for both responses is the pooled higher-order interaction term at the experimental-run level.

Whether the material effect operates through cutting force was tested by hierarchical regression: with cutting force, cutting speed and feed in the model, the incremental contribution of the material variables was assessed by partial F tests.

The six tests carrying the dissociation claim were defined as the **primary family**, and Bonferroni and Benjamini–Hochberg (BH) corrections were applied to this family. Confidence intervals for effect sizes were obtained by resampling observations (bootstrap, B = 4000).

The built-up-edge grades used in the analysis are the author's. A preliminary set of grades produced with AI assistance (Sect. 2.5) is retained for comparison, and the agreement between the two sets is quantified by Cohen's κ and linearly weighted κ. This is a **consistency check, not a measure of observer-independent reliability** (Sect. 4.1).

Taguchi signal-to-noise ratios were computed on the smaller-is-better criterion:

$$S/N = -10 \cdot \log_{10}\left((1/n) \Sigma y_i^{\,2} \right)$$

Regression models were compared by **leave-one-out cross-validation (LOOCV)**. In a sample as small as n = 36, R^2 alone is not an adequate criterion; LOOCV reveals the point at which model complexity begins to degrade predictive performance.

In addition to the explicitly parameterised models, three flexible learners were tested: a regression tree (CART, sum-of-squares criterion), a random forest (with bootstrap

sampling and variable subsetting) and k-nearest neighbours. All three were evaluated by the same LOOCV procedure on an identical input set.

All analyses were performed with scripts written without external statistical or machine-learning libraries, so that the results can be reproduced exactly.

2.5 Use of AI tools

A large language model (Anthropic Claude) was used as an assistant throughout the analysis and preparation of this manuscript. Its contribution was as follows.

- **Analysis code.** The scripts implementing the analysis of variance, the bootstrap resampling, the leave-one-out cross-validation and the regression tree, random forest and k-nearest-neighbour learners were written with AI assistance. All numerical results were regenerated and checked by the author against the raw data.
- **Figures.** The scripts generating Figs. 2–7 were written with AI assistance; the figures are produced directly from the data file.
- **Text.** The manuscript was drafted with AI assistance and revised by the author.
- **Literature.** Candidate references were identified with AI assistance; every bibliographic entry was verified by the author against Crossref.
- **Preliminary built-up-edge scoring.** A first, provisional set of ordinal built-up-edge grades was produced with AI assistance from the SEM images. The scoring used in the analysis is the author's own (Sect. 4.1).

The author conceived the research question, provided and verified the experimental data, performed the built-up-edge scoring used in the analysis, checked every numerical result, and takes full responsibility for the accuracy and integrity of the work. The AI tool is not an author and has no accountability for the content.

2.6 Figure preparation

The numerical figures (Figs. 2–7) were produced directly from the raw data file by a single script; any change to the dataset regenerates all of them. This removes the possibility of an inconsistency between figure values and text values arising from manual transcription. The figures were produced in scalable vector format.

No manipulation was applied to the image content of the photographic figures (Figs. 1, 8 and 9): no contrast, brightness, sharpness or colour adjustment was made, and no region was removed, added or rearranged. Two operations were performed:

1. In the SEM images (Fig. 8), the **institution name and instrument manufacturer in the information bar were masked**. The measurement information — accelerating voltage, working distance, detector type, magnification, field of view, date and the **scale bar** — was left intact, so that the reader can verify the scale and acquisition conditions of the images. The image area itself was not touched.

2. In the chip photographs (Fig. 9), the empty background at the bottom of the frame was cropped to use the page area efficiently. The chip samples and the scale rule are entirely within the frame.

---

3 Results

3.1 The double dissociation

The principal finding of the study is shown in Fig. 2.

Strontium markedly increases the cutting force, while no effect on surface roughness is detectable. The mean cutting force rises from 20.6 N in the strontium-free groups to 29.7 N in the strontium-bearing groups (+44 %; $F(1,16) = 32.30$; $p < 0.001$). In the same comparison the surface roughness goes from 2.98 µm to 2.93 µm; the effect is not statistically detectable ($F(1,16) = 0.22$; $p = 0.65$).

The copper–tin addition does exactly the reverse. Surface roughness rises from 2.18 µm in the copper–tin-free groups to 3.73 µm in the copper–tin-bearing groups (+71 %; $F(1,16) = 182.52$; $p < 0.001$). In the same comparison the cutting force goes from 25.2 N to 25.0 N; the effect is not statistically detectable ($F(1,16) = 0.01$; $p = 0.94$).

> **Fig. 2** Double dissociation: two addition elements, two different responses. Upper panels: group means with standard errors. Lower panels: adjusted effects with 95 % bootstrap confidence intervals (B = 4000); grey indicates an interval containing zero

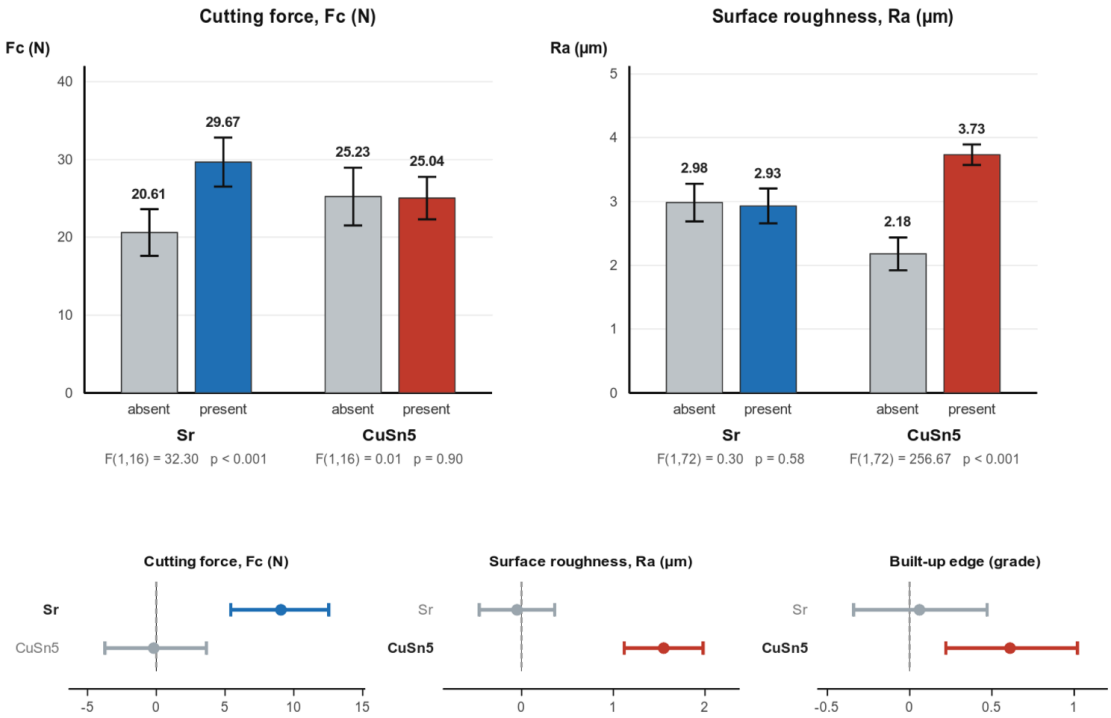


Fig. 2

The pattern is a **double dissociation** in the descriptive sense: each of two factors has a large effect on one response and no detectable effect on the other, both measured in the same dataset under the same conditions. The term is used here to describe the observed pattern of *response-specific dominant effects*, not to assert that the two additions act through mutually independent physical mechanisms — an assertion the design cannot support (Sect. 3.2).

The **completeness** of the dissociation was tested separately. With cutting force, cutting speed and feed controlled:

Term added to the model	Effect on Ra
Copper–tin (binary)	$F(1,31) = 55.13$ · **$p < 0.000001$**
Strontium (binary)	$F(1,31) = 0.10$ · $p = 0.76$
Full material dummies (3 df)	$F(3,29) = 18.32$ · **$p < 0.000001$**
Full dummies, with copper–tin already present	**$F(2,29) = 0.61$ · $p = 0.55$**

The last row is informative: **once the copper–tin variable enters the model, material group makes no further contribution to surface roughness.** Within the present model and experimental range, therefore, the material-group contribution to Ra is accounted for by the CuSn5 term alone; no separate strontium contribution is detectable.

The same test gives the reverse result for cutting force: adding strontium yields $F(1,32) = 26.38$ ($p < 0.001$), whereas adding copper–tin yields $F(1,32) = 0.01$ ($p = 0.94$).

3.1.1 Bounding the null effects

A double dissociation claim cannot rest on "not significant"; the effect must be shown to be **small**. Otherwise the finding is an *absence of evidence* rather than *evidence of absence*. Point estimates and 95 % bootstrap confidence intervals (B = 4000) were therefore computed for every effect (Table 2).

Table 2 Adjusted effect sizes and 95 % confidence intervals. Model: y ~ V + f + CuSn5 + Sr

Response	Factor	Effect	95 % CI	Zero
Cutting force (N)	**Sr**	**+9.06**	[+5.41, +12.54]	outside
Cutting force (N)	CuSn5	−0.19	[−3.73, +3.65]	inside
Surface roughness (µm)	Sr	−0.05	[−0.46, +0.36]	inside
Surface roughness (µm)	**CuSn5**	**+1.55**	[+1.12, +1.98]	outside

The confidence intervals place upper bounds on the null effects:

- **The strontium effect on surface roughness is at most ±0.46 µm** — approximately **29 %** of the copper–tin effect (+1.55 µm).
- **The copper–tin effect on cutting force is at most ±3.73 N** — approximately **41 %** of the strontium effect (+9.06 N).

Both null effects are therefore confined to an interval smaller than half the magnitude of the opposing factor's effect. This bounds the null effects as *small relative to the corresponding non-null effects*; it does not establish formal statistical equivalence, which would require a pre-specified equivalence margin. What the intervals do rule out is that the pattern arises solely from insufficient measurement sensitivity.

The same criterion is applied to built-up edge in Sect. 4.1, where it is **not** met; because that null effect cannot be bounded, the double dissociation claim is confined to cutting force and surface roughness.

3.1.2 Multiple comparisons

Many tests were performed in this study. The **six tests carrying the dissociation claim** (two factors × three responses) were defined as the primary family, and the correction was applied to that family (Table 3). All three significant results survive the Bonferroni correction at α = 0.05.

Table 3 Primary test family and multiple-comparison correction (m = 6)

Test	F	Raw p	Bonferroni p	BH q
CuSn5 → Ra	56.69	1.4×10^{-8}	$\mathbf{8.5 \times 10^{-8}}$	8.5×10^{-8}

Test	F	Raw p	Bonferroni p	BH q
Sr → Fc	26.38	1.3×10^{-5}	$\mathbf{8.0 \times 10^{-5}}$	4.0×10^{-5}
CuSn5 → BUE	9.31	4.6×10^{-3}	$\mathbf{2.7 \times 10^{-2}}$	9.1×10^{-3}
Sr → BUE	0.06	0.809	1.00	1.00
Sr → Ra	0.22	0.648	1.00	1.00
CuSn5 → Fc	0.01	0.935	1.00	0.935

3.1.3 Robustness: eight disputed force values

For eight of the cutting force values, two different records exist in the study documentation (Sect. 5). Whether the main finding depends on this choice was tested across three data variants (Table 4).

Table 4 Sensitivity of the main finding to data variant

Variant	Sr → Fc	p	CuSn5 → Fc	p	CuSn5 → Ra	p	Sr → Ra	p
Thesis values (n = 36)	**+9.06 N**	1×10^{-5}	−0.19 N	0.94	**+1.55 µm**	1×10^{-8}	−0.05 µm	0.88
Alternative record (n = 36)	**+8.03 N**	9×10^{-5}	+1.91 N	0.41	**+1.55 µm**	1×10^{-8}	−0.05 µm	0.88
Disputed 8 excluded (n = 28)	**+8.92 N**	3×10^{-4}	+0.61 N	0.49	**+1.65 µm**	1×10^{-6}	−0.12 µm	0.76

The same structure is preserved in all three variants: strontium raises the cutting force by 8–9 N and remains significant at $p < 0.001$, while the copper–tin effect on cutting force is not significant in any variant. The main finding does not depend on which record the disputed values are read from.

3.2 Variance decomposition

The analysis of variance confirms this picture quantitatively (Tables 5 and 6, Fig. 3). Table 5 gives the decomposition for cutting force and Table 6 that for surface roughness.

Table 5 Analysis of variance for cutting force Fc (single observation per cell; error estimated by pooling higher-order interactions)

Source	SS	df	MS	F	p	Share of total SS (%)
Feed	4156.35	2	2078.18	90.85	< 0.001	**63.6**
Cutting speed	758.06	2	379.03	16.57	< 0.001	11.6
Sr	738.93	1	738.93	32.30	< 0.001	**11.3**
CuSn5 × Feed	158.20	2	79.10	3.46	0.056	2.4
Cutting speed × Feed	149.07	4	37.27	1.63	0.215	2.3
Sr × CuSn5	114.13	1	114.13	4.99	0.040	1.7
CuSn5 × Cutting speed	74.25	2	37.13	1.62	0.228	1.1
Sr × Feed	22.97	2	11.49	0.50	0.614	0.4
Sr × Cutting speed	1.16	2	0.58	0.03	0.975	0.0
CuSn5	**0.34**	**1**	**0.34**	**0.01**	**0.904**	**0.0**
Pooled error	365.98	16	22.87			5.6
Total	**6539.46**	**35**				**100**

Table 6 Analysis of variance for surface roughness Ra at the experimental-run level (n = 36 run means; pooled error)

Source	SS	df	F	p	Share of total SS (%)
CuSn5	21.69	1	182.52	< 0.001	**43.6**
Feed	13.47	2	56.66	< 0.001	**27.0**
CuSn5 × Feed	5.37	2	22.61	< 0.001	10.8
Cutting speed	3.50	2	14.71	< 0.001	7.0
Cutting speed × Feed	2.13	4	4.48	0.013	4.3
CuSn5 ×	0.79	2	3.32	0.062	1.6

Source	SS	df	F	p	Share of total SS (%)
Cutting speed					
Sr × CuSn5	0.48	1	4.02	0.062	1.0
Sr × Feed	0.23	2	0.97	0.402	0.5
Sr × Cutting speed	0.22	2	0.94	0.410	0.4
Sr	**0.03**	**1**	**0.22**	**0.648**	**0.1**
Pooled error	1.90	16			3.8
Total	**49.80**	**35**			**100**

Choice of experimental unit. The three roughness readings taken from each machined region are repeated measurements on the *same* machining run, not independently machined specimens. Treating them as independent replicates would inflate the error degrees of freedom and overstate the precision of the F tests. The analysis in Table 6 is therefore conducted at the **experimental-run level** (n = 36 cell means), with the error term estimated by pooling higher-order interactions exactly as for cutting force. The repeated readings are used only to characterise measurement precision: the mean within-run standard deviation of the three readings is 0.386 μm, against a between-run standard deviation of 1.193 μm, so measurement noise accounts for a small fraction of the total variation.

Analysing the 108 individual readings with a pure-error term (df = 72) instead does not alter the principal conclusions — CuSn5 remains dominant (F = 256.67), feed second (F = 79.70) and Sr null (F = 0.30, p = 0.583) — but it does inflate two secondary interactions above the significance threshold. In the run-level analysis reported here, CuSn5 × cutting speed (p = 0.062) and Sr × CuSn5 (p = 0.062) are **not** significant, whereas the reading-level analysis returns p = 0.012 and p = 0.020 respectively. The more conservative run-level result is adopted throughout, and no claim in this paper rests on those two terms.

Fig. 3 Share of the total sum of squares attributable to each factor (%) — cutting force compared with surface roughness. In an unreplicated factorial design these shares describe the decomposition of the observed sum of squares and should not be read as population variance explained

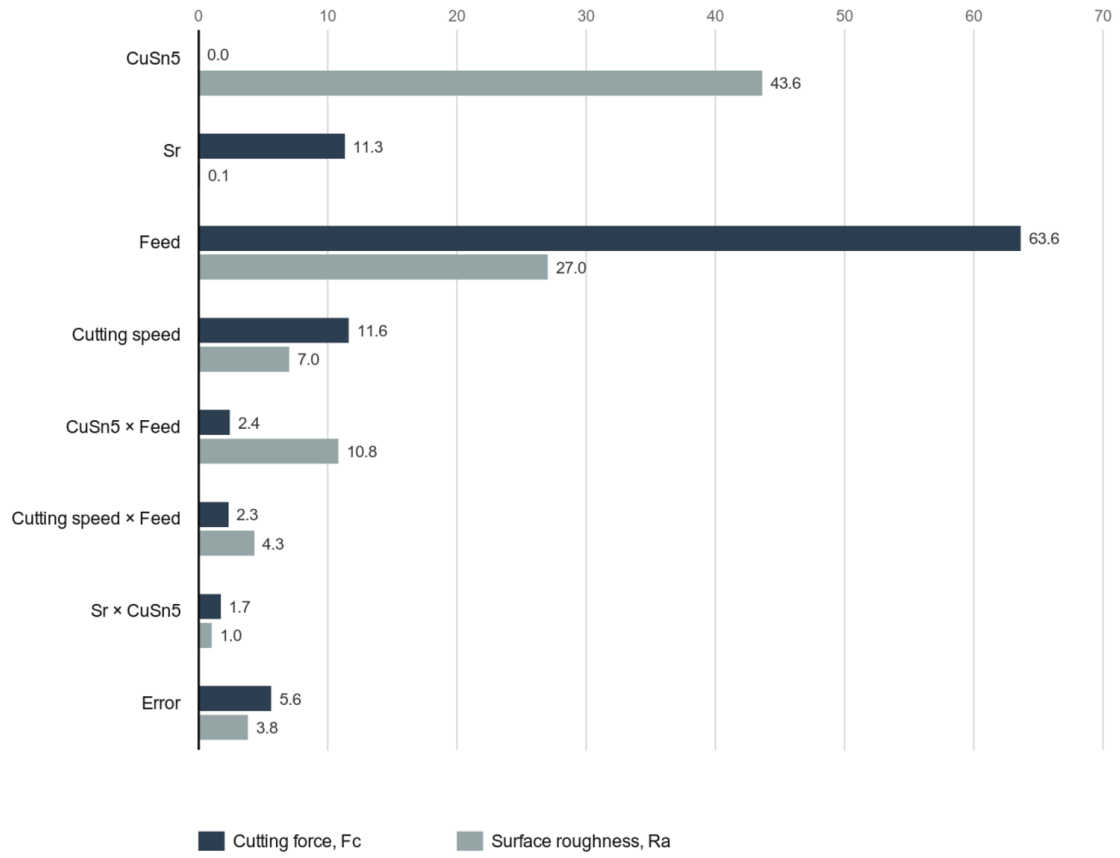


Fig. 3

The dissociation becomes visible in the numbers when the first rows of the two tables are compared. For cutting force, Sr accounts for 11.3 % and CuSn5 for 0.0 %; for surface roughness, CuSn5 accounts for 38.8 % and Sr for 0.0 %.

Among the process parameters, **feed is strong for both responses** but occupies a different position: it is the single dominant factor for cutting force (63.6 %), whereas for surface roughness it comes second to copper–tin (24.1 %). The contribution of cutting speed is limited for both responses.

3.2.1 The Sr × CuSn5 interaction on cutting force

The decomposition into Sr and CuSn5 components is *orthogonal by construction*, because the design is balanced. Orthogonal coding is a property of the design matrix, however, and does not imply that the two additions act independently in the material. For cutting force the analysis returns a significant Sr × CuSn5 interaction ($F(1,16) = 4.99$; $p = 0.040$), and the simple effects should therefore be reported:

	CuSn5 absent	CuSn5 present	Sr simple effect
Sr absent	18.92 N	22.29 N	—
Sr present	31.54 N	27.79 N	—

	CuSn5 absent	CuSn5 present	Sr simple effect
Sr simple effect	**+12.62 N**	**+5.50 N**	interaction −7.12 N

The strontium effect is large and positive under both conditions; the interaction reduces its magnitude by rather more than half when CuSn5 is also present, but does not reverse or abolish it. The appropriate description is therefore **response-specific dominant effects**, not mutually independent mechanisms. A possible physical reading is that the two additions may interact through their effects on the eutectic structure: the source work notes that the CuSn5 addition reduces the effectiveness of modification, which would be expected to blunt the strontium effect where both are present. The present design does not test this directly.

The main-effects plots (Fig. 4) show the same structure graphically: the material panel traces a moderate path for cutting force but a pronounced zigzag for surface roughness — and that zigzag arises precisely from the elevation of the copper–tin-bearing groups B and D.

Fig. 4 Main-effects plots

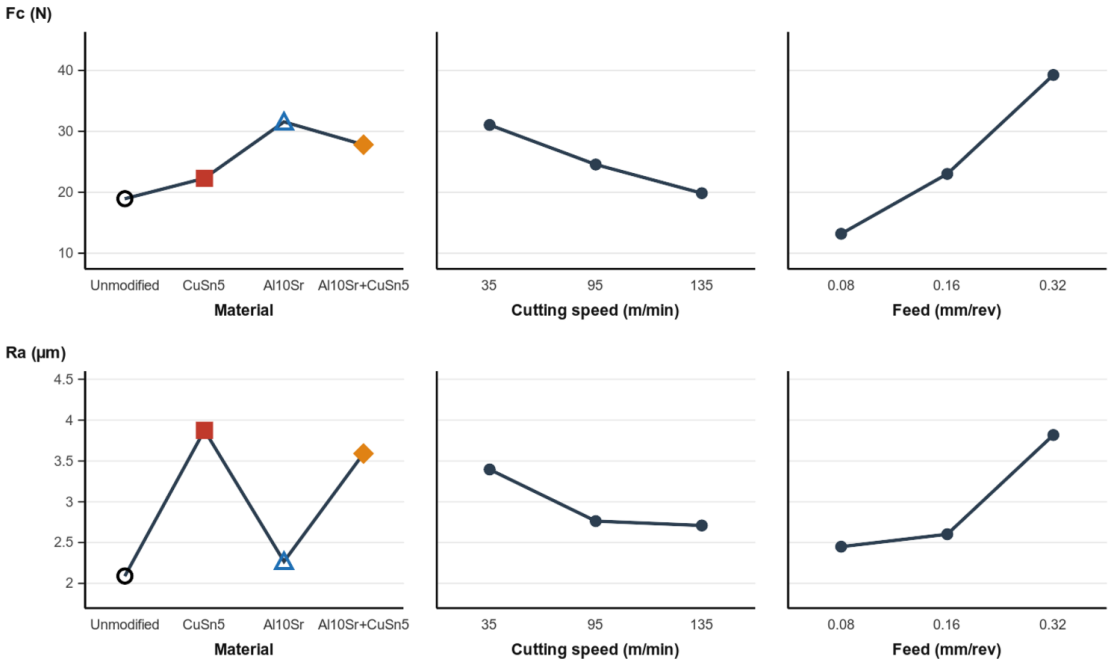


Fig. 4

3.3 The copper–tin × feed interaction

The third-largest term for surface roughness is the CuSn5 × feed interaction (9.6 %; $p < 0.001$). Figure 5 shows what this means.

Fig. 5 Material × feed interaction — Ra

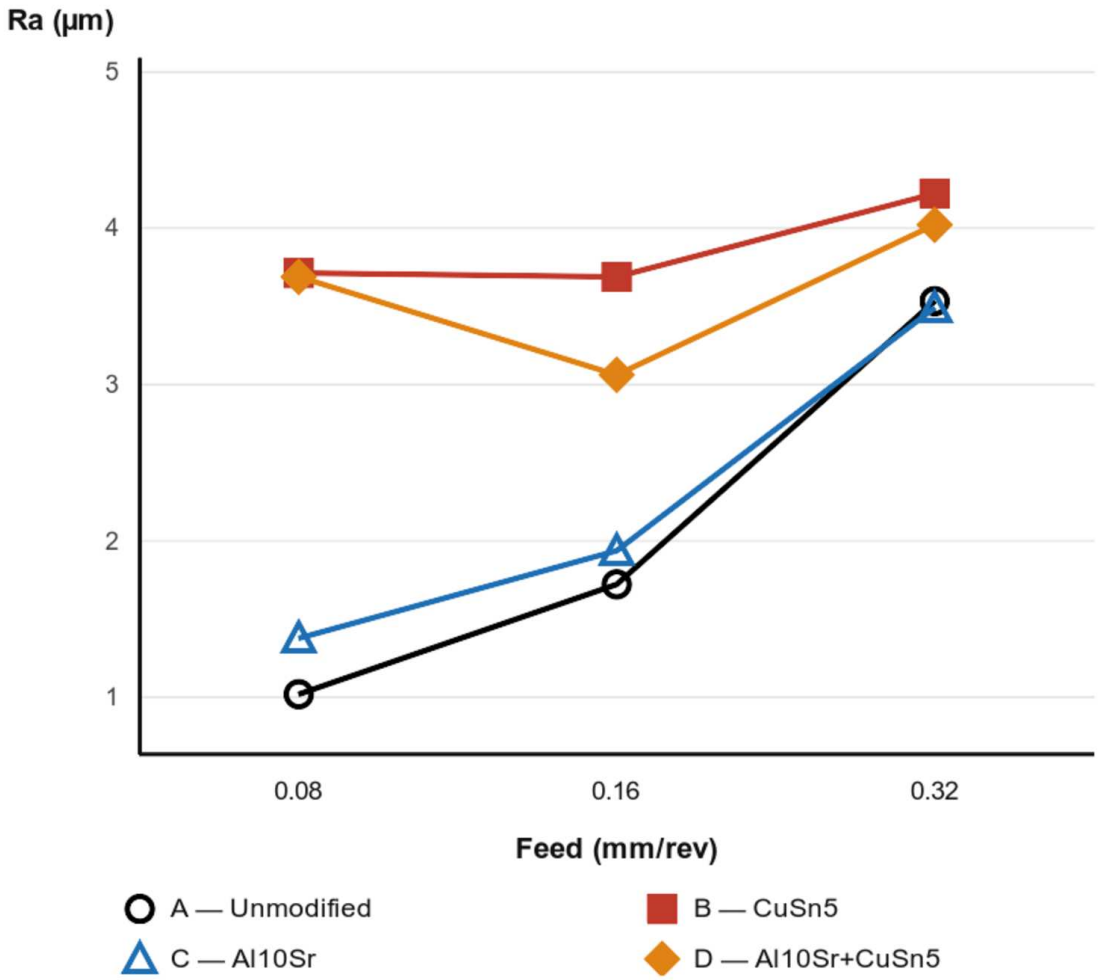


Fig. 5

The four curves separate into **two families**. Groups A and C, which contain no copper–tin, give a very good surface at low feed and deteriorate steeply as feed increases. Groups B and D, which contain copper–tin, **begin at high roughness even at the lowest feed** and are almost insensitive to feed (Table 7).

Table 7 Group × feed cell means, Ra (µm)

Group	f = 0.08	f = 0.16	f = 0.32	Ratio (0.32 / 0.08)
A — unmodified	**1.02**	1.72	3.53	**3.46 ×**
C — Al10Sr	**1.38**	1.94	3.49	**2.53 ×**
B — CuSn5	3.71	3.69	4.22	1.14 ×
D — Al10Sr+CuSn5	3.69	3.06	4.02	1.09 ×

The practical consequence is that **surface quality cannot be gained by reducing the feed in copper–tin-bearing alloys.** Reducing the feed from 0.32 to 0.08 mm/rev lowers the roughness by a factor of 3.5 in group A and 2.5 in group C; in groups B and D the change is below 15 %. Here the limit on surface quality is set not by the process parameter but by the material.

3.4 Force-component ratio and surface roughness

The cutting force itself is a weak predictor of surface roughness (r = +0.497). The ratio of feed force to cutting force (Ff/Fc), by contrast, shows a **stronger and inverse relationship** (r = −0.661) (Fig. 6).

Relationship	r
Ff/Fc – Ra	**−0.661**
Fc – Ra	+0.497
Ff – Ra	+0.211

Fig. 6 Relationship of surface roughness to force indicators: **a** Ff/Fc ratio, **b** cutting force

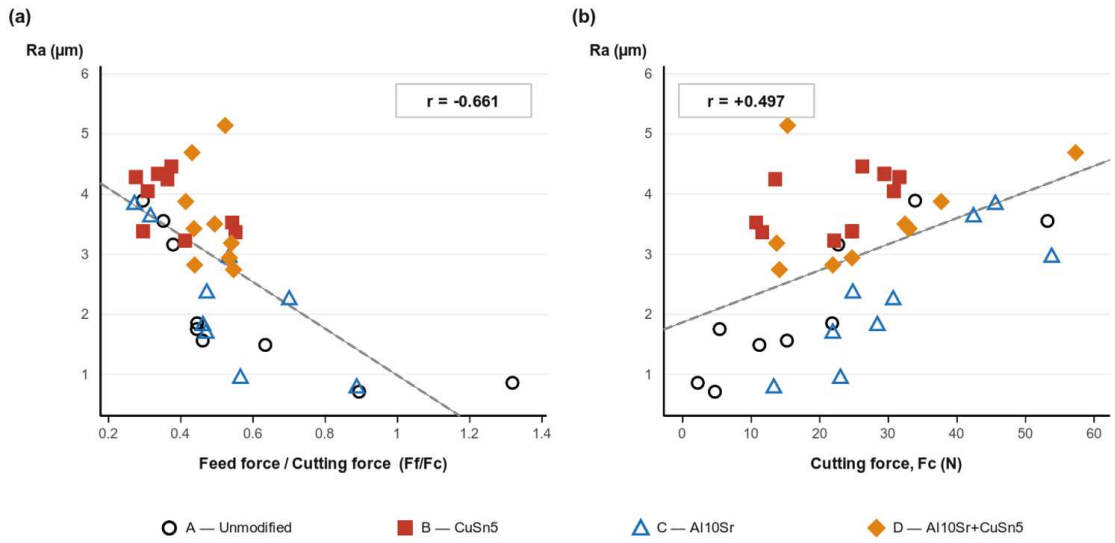


Fig. 6

A high Ff/Fc ratio goes with a good surface and a low ratio with a poor one. The group means are consistent: Ff/Fc = 0.550 in the copper–tin-free groups and 0.434 in the copper–tin-bearing groups (with cutting force, cutting speed and feed controlled, $F(1,31) = 4.48$; $p = 0.042$). Strontium has no detectable effect on this ratio ($p = 0.41$).

A raw correlation is not sufficient to establish that the ratio carries information beyond its constituents, since Ff/Fc is constructed from Fc and Ff and both are generated by the same cutting event. The ratio was therefore added to progressively richer models (Table 8).

Table 8 Incremental contribution of Ff/Fc to the prediction of Ra

Base model	+ Ff/Fc	Coefficient
V + f	$F(1,32) = 10.97$ · **$p = 0.0023$**	−2.99
V + f + Fc	$F(1,31) = 10.62$ · **$p = 0.0027$**	−3.00
V + f + material (Sr, CuSn5)	$F(1,30) = 5.54$ · **$p = 0.025$**	−1.50
V + f + material + Fc	$F(1,29) = 4.99$ · **$p = 0.033$**	−1.47
For comparison: V + f + material, **+ Fc**	$F(1,30) = 0.40$ · $p = 0.53$	—

Ff/Fc retains a significant negative contribution after cutting speed, feed, material and the cutting force itself are all controlled. The cutting force, by contrast, adds nothing once material is in the model ($p = 0.53$). Within this dataset the ratio therefore carries information about surface roughness that its own numerator and denominator do not. It should be read as an **indicator of the contact and shear state at the tool–workpiece interface** rather than as an independent physical driver: being a composite of the two measured force components, it summarises how the cutting load is partitioned rather than exerting an effect of its own. Whether it is a better predictor in general cannot be established from a single alloy system.

Table 9 Means by material group

Group	Fc (N)	Ff (N)	Ff/Fc	Ra (µm)	BUE (0–3)
A — unmodified	18.9	7.8	0.580	**2.09**	1.89
B — CuSn5	22.3	7.9	**0.384**	**3.88**	2.33
C — Al10Sr	**31.5**	15.1	0.520	2.27	1.78
D — Al10Sr+CuSn5	27.8	13.0	0.484	3.59	2.56

The Ff/Fc column is the mean of the per-run ratios, not the ratio of the means.

Table 9 shows the double dissociation at group level as well. **Al10Sr produces the highest cutting force yet gives the second-best surface; CuSn5 produces the second-lowest force yet the worst surface.** The common intuition about the force–surface relationship does not hold in these data.

3.5 Taguchi analysis

The signal-to-noise analysis is summarised in Table 10.

Table 10 Signal-to-noise ratios (smaller-is-better) and optimum levels

Factor	**Fc** optimum	Δ (dB)	**Ra** optimum	Δ (dB)
Material	B — CuSn5	3.12	A — unmodified	4.37
Cutting speed	135 m/min	3.66	135 m/min	1.77
Feed	**0.08 mm/rev**	**8.95**	**0.16 mm/rev**	2.93

Feed has the single strongest effect in the study on cutting force (Δ = 8.95 dB), with its optimum at the lowest level. For surface roughness the optimum is at the **intermediate** level — a consequence of the two-family structure in Fig. 5: the lowest feed is advantageous only in the copper–tin-free groups, and this advantage is diluted in the overall mean.

The material row is particularly noteworthy. On the cutting-force criterion the best material by S/N is **B (CuSn5)**, whereas the material with the lowest mean cutting force is A (18.9 N; B gives 22.3 N). This is not a contradiction but follows from the definition of the S/N criterion: group A gives a lower mean but spreads over a far wider range (2.2–53.2 N), whereas B remains within a narrow band (10.7–31.6 N). The Taguchi criterion penalises the mean and the variability jointly. **The "best" material in the same dataset therefore changes with the criterion** — a concrete illustration of the limits of single-response optimisation.

3.6 Model comparison

Table 11 Comparison of regression models by cross-validation

Model	p	R^2	adj. R^2	RMSE	**LOOCV**
Cutting force (N)					
Linear (V, f)	3	0.750	0.735	6.74	7.44
Linear + Sr + CuSn5	5	0.863	0.845	4.99	5.88
Linear + material dummies	6	0.880	0.860	4.66	**5.74**
Linear + Sr + CuSn5 + CuSn5×f	6	0.874	0.853	4.79	5.88
Quadratic (RSM)	6	0.772	0.734	6.43	7.85
RSM + Sr + CuSn5	8	0.885	0.857	4.57	6.00
RSM + material	9	**0.903**	0.874	4.20	5.83

Model	p	R^2	adj. R^2	RMSE	**LOOCV**
dummies					
RSM + Sr + CuSn5 + CuSn5×f	9	0.896	0.865	4.34	5.96
Surface roughness (µm)					
Linear (V, f)	3	0.319	0.277	0.97	1.06
Linear + Sr + CuSn5	5	0.755	0.723	0.58	0.68
Linear + material dummies	6	0.764	0.725	0.57	0.70
Linear + Sr + CuSn5 + CuSn5×f	6	0.858	0.835	0.44	0.54
Quadratic (RSM)	6	0.364	0.258	0.94	1.13
RSM + Sr + CuSn5	8	0.800	0.750	0.53	0.68
RSM + material dummies	9	0.810	0.753	0.51	0.69
RSM + Sr + CuSn5 + CuSn5×f	9	**0.904**	**0.875**	**0.37**	**0.50**

Three points in Table 11 are important.

First, for cutting force the model with the highest R^2 does not give the best prediction. The RSM + material dummies model achieves the highest fit at $R^2 = 0.903$, yet its LOOCV error is worse than that of the simpler linear + material model (5.74 → 5.83 N). Fitting nine parameters to 36 observations produces overfitting. In the machining literature, model performance is usually reported by R^2 alone; this example shows that in small samples this can be misleading.

Second, for surface roughness the decisive element is not the model order but a single interaction term. Adding the **CuSn5 × feed** product to the linear model lowers the LOOCV error from 0.68 to 0.54; adding the same term to the RSM lowers it from 0.68 to **0.50**. This is the direct numerical counterpart of the two-family structure documented in Sect. 3.3.

Third, the two responses require different representations. For surface roughness the two-parameter binary representation (Sr + CuSn5) predicts better than the three-parameter full dummy representation (0.68 vs 0.70; 0.50 in the interaction version). For cutting force the full dummy representation retains a small advantage (5.74 vs 5.88) — consistent with the Sr × CuSn5 interaction being significant for cutting force ($p = 0.040$) and negligible for surface roughness.

Power-law models are given for comparison with the literature:

$$Fc = 524.7 \cdot V^{(-0.375)} \cdot f^{(+0.871)} \quad Ra = 16.17 \cdot V^{(-0.220)} \cdot f^{(+0.466)}$$

The feed exponent of 0.871 for cutting force is consistent with the typical range in the machining literature (≈0.75–1.0) and supports the physical consistency of the measurement set. The explanatory power of the power law for surface roughness is low ($R^2 = 0.315$ on the log scale) — an expected result, since this model does not contain the material variable and, as shown in Sect. 3.1, material is the largest determinant of Ra.

The extent to which the selected models reproduce the observed values is shown in Fig. 7.

Fig. 7 Observed versus model-predicted values. The dashed line is the line of identity. **a** cutting force, linear + material model; **b** surface roughness, RSM + material model

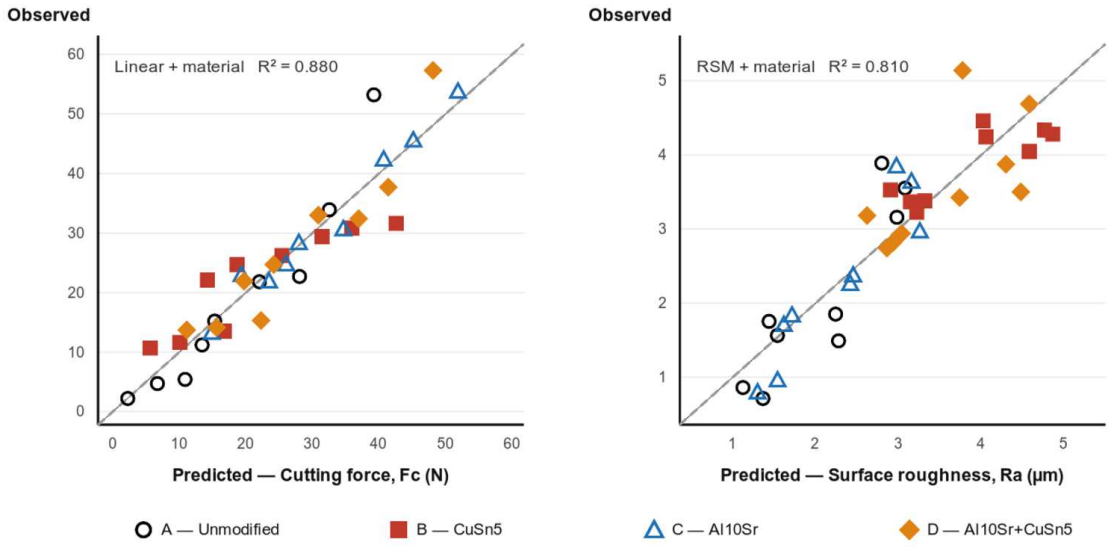


Fig. 7

3.7 Do flexible learners offer an advantage in this sample?

Predictive models built with neural networks, fuzzy logic and ensemble methods are increasingly common in the machining literature. Whether such methods outperform explicitly parameterised models in a design as small as n = 36 was tested directly: a regression tree (CART), a random forest (500 trees) and k-nearest neighbours were fitted to the same four inputs (V, f, Sr, CuSn5) and evaluated by the same LOOCV procedure (Table 12).

Table 12 Flexible learners compared with the explicitly parameterised model (LOOCV)

Model	Fc LOOCV	Ra LOOCV
Linear + Sr + CuSn5 (5 parameters)	**5.88**	0.68
Regression tree (depth 5)	8.66	**0.49**
Random forest (500 trees)	7.52	0.63
k-nearest neighbours (k = 3)	9.30	0.70
RSM + Sr + CuSn5 + CuSn5×f (9 parameters)	5.96	**0.50**

For cutting force the flexible learners fall clearly behind the five-parameter linear model (5.88 N against 7.52 N for the best of them). For surface roughness the regression tree does better than the linear model (0.49 versus 0.68), but inspection shows why: its first split is on the copper–tin variable, with a subsequent split on feed only in the copper–tin-free branch — exactly the interaction documented in Sect. 3.3. Writing that interaction into the parametric model as an explicit product term closes the gap (0.50 versus 0.49).

At this scale of design, therefore, flexible learners are useful as tools of *discovery* rather than of prediction: the structure the tree found can be named, and the named version delivers equivalent predictive performance with interpretable coefficients and significance tests. Full results for all model variants and depths are given in Online Resource 1.

---

4 Discussion

4.1 The built-up-edge hypothesis and its testing

The dissociation shown in Sect. 3.1 raises a question of mechanism: how does the copper–tin addition degrade surface quality without changing the cutting force?

The first candidate is **built-up-edge (BUE) formation**. Adhesion of material at the tool–chip interface is common in the machining of aluminium alloys; the deposit breaks away periodically and damages the machined surface. The fall in Ff/Fc reported in Sect. 3.4 can also be read in this direction, since the ratio is sensitive to the contact regime at the interface.

This hypothesis was tested directly. SEM images of the inserts taken after the experiments were scored on an **ordinal scale from 0 to 3** according to the volume of the deposit and the degree to which the cutting edge was covered (Fig. 8). The scale runs from a thin surface film with the cutting edge retaining its sharpness (grade 1) to the edge geometry being wholly buried under a layered mass (grade 3).

Fig. 8 Definition of the built-up-edge grading scale. Group A (unmodified), V = 95 m/min; left to right f = 0.08 · 0.16 · 0.32 mm/rev (experiments 4, 5, 6). **Grade 1:** thin surface film, cutting edge retains sharpness. **Grade 2:** localised moderate deposit at the nose, edge line partly covered. **Grade 3:** layered mass concealing the edge geometry. SEM, secondary-electron detector, 100× magnification, 20 kV, field of view 2.30 mm; scale bar 500 µm. Only the institution name and instrument brand have been masked in the information bar (Sect. 2.6); the image content is unaltered

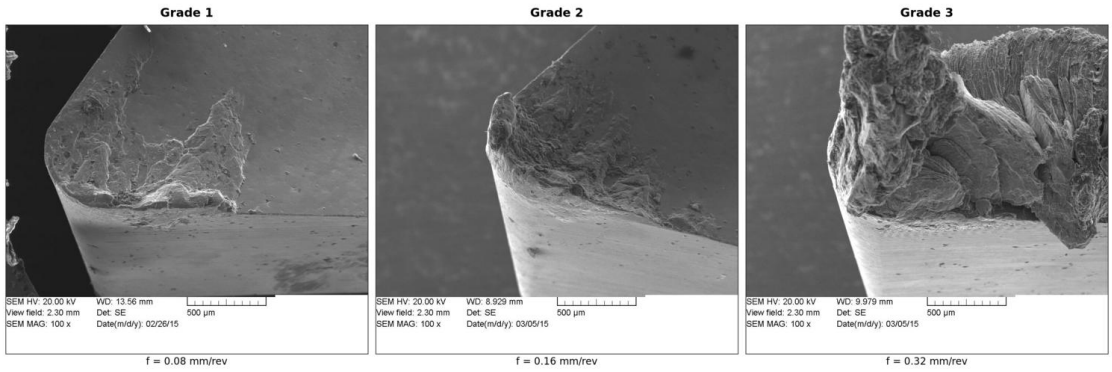


Fig. 8

Two sets of grades exist for these images. A **preliminary set was produced with AI assistance** from the images (Sect. 2.5); the **author then graded all images**, and it is the author's grades that are used in every analysis reported below. Comparing the two sets gives an **agreement with an AI-assisted preliminary scoring**, reported here as a consistency check and not as a reliability statistic:

- Exact agreement: **24 of 30 comparable images (80 %)**
- All disagreements within **±1 grade**; no image showed a 1 ↔ 3 jump
- Cohen's κ = **0.693**; linearly weighted κ = **0.764**

Two qualifications are necessary. First, this is **not** inter-observer agreement between two independent human assessors, and it should not be read as such. Second, the preliminary grades were visible in the working file when the author graded the images, so the comparison is not blinded and the agreement figure is likely to be optimistic. The comparison indicates only that the ordinal categories can be applied consistently to these images. It is **not evidence of observer-independent reliability**, and the κ values should not be read as such.

Table 13 Rank correlations of built-up-edge grade with other variables (Spearman ρ, n = 36)

Comparison	ρ	p
BUE – Feed	**+0.578**	**0.0002**
BUE – Cutting force	**+0.501**	**0.0018**
BUE – Ra	**+0.469**	**0.0039**

Comparison	ρ	p
BUE – Ff/Fc	**−0.385**	**0.0204**
BUE – Cutting speed	−0.009	0.960

Built-up-edge severity correlates significantly with feed, cutting force and surface roughness, and its correlation with the Ff/Fc ratio is negative as expected. The scale is not merely noise.

With cutting speed and feed controlled, copper–tin raises the built-up-edge grade ($F(1,32) = 9.31$; $p = 0.005$) while strontium does not ($F(1,32) = 0.06$; $p = 0.81$); once copper–tin is in the model, the full material dummies add nothing ($F(2,30) = 0.37$; $p = 0.69$). The mean grade is 2.44 in the copper–tin-bearing groups and 1.83 in the others; the strontium-bearing and strontium-free groups are indistinguishable (2.17 and 2.11).

This dissociation is, however, **weaker** than those for cutting force and surface roughness, and this must be stated explicitly when the confidence-interval criterion of Sect. 3.1.1 is applied. The adjusted effects and 95 % confidence intervals are **+0.61 grade [+0.22, +1.02]** for copper–tin and **+0.06 grade [−0.34, +0.47]** for strontium. The upper bound placed on the strontium null (0.47) is **78 %** of the copper–tin effect, whereas the corresponding ratio is 41 % for cutting force and 29 % for surface roughness.

What can be said for built-up edge is therefore: **copper–tin has been shown to increase built-up edge; strontium has not been shown not to.** This is a one-directional finding rather than a full dissociation. The three-level ordinal scale has limited resolution, and a finer quantification — for example profilometric measurement of deposit volume — would remove this limitation.

A stronger test is **conditional association**: if the material effect on surface roughness operated largely *through* built-up edge, that effect should attenuate substantially when the BUE score enters the model. This is an attenuation test, not a formal mediation analysis — built-up edge and the machined surface are generated within the same cutting event and are not temporally separated, so the causal ordering required by mediation analysis cannot be established here.

Model	Copper–tin effect on Ra
Fc + V + f → + CuSn5	$F(1,31) = 55.13$
Fc + V + f + **BUE** → + CuSn5	$F(1,30) =$ **48.81**

The effect weakens by only **11 %.** The same test with full material dummies gives a comparable result ($F(3,29) = 18.32 \rightarrow F(3,28) = 16.00$).

The association between the CuSn5 addition and surface roughness is therefore only weakly attenuated by the measured built-up-edge score. The CuSn5 addition raises both built-up edge and surface roughness, but the measured BUE score accounts for little of the roughness effect. A reading consistent with the data is that the two responses are **parallel consequences of a common material-related cause**; the data neither establish

such a common cause nor exclude built-up edge being part of the mechanism in a way the ordinal score failed to capture.

This weakens, without formally refuting, the initial formulation — that surface degradation arises chiefly from the detachment of built-up edge. On the present evidence built-up edge is better regarded as an accompanying symptom than as the principal route.

The limits of the finding must be stated: the grades used are those of a single assessor, applied at a single magnification, and no observer-independent reliability was established (Sect. 5). An insensitive measure can also fail to show attenuation. The result should therefore be read as evidence that *the measured BUE score* does not account for the roughness effect, not as proof that built-up edge plays no part in it.

4.2 An alternative mechanism: a discrete hard second phase

A second explanation, more consistent with the data, is **visible directly in the microstructure.** In Fig. 1 the copper–tin-bearing groups B and D contain **discrete, angular, dark second-phase particles** that are absent in A and C; in group B the eutectic silicon has additionally shortened and become blocky. During cutting, hard and discontinuous particles of this kind fracture or are torn from the matrix; the resulting voids and tear marks are transferred directly to the machined surface.

As noted in Sect. 2.2, the phase of these particles cannot be determined at optical magnification. The composition and the literature suggest Al_2Cu-type copper intermetallics as a plausible candidate; Basavakumar and co-workers report $CuAl_2$ particles in the interdendritic regions of an Al-12Si-3Cu alloy [19]. It must be stressed that the experiment identifies the effect of the **CuSn5 master-alloy treatment**, not the isolated effect of copper: tin (0.067–0.074 wt%) was introduced together with copper and was never varied independently. Tin influences chip breakability and tribological behaviour, so its contribution to the observed effects cannot be separated from that of copper in this design. However, the dark phases in an etched Al-Si section are predominantly silicon, and **neither EDS nor backscattered-electron imaging was performed in this study.** The mechanism is therefore formulated independently of phase identity: what matters is that the addition introduces a discrete, hard second phase.

The hardness values in Table 1 support this reading. The copper–tin addition raises hardness markedly (A → B: 85.7 → 90.4 HB; C → D: 86.2 → 99.2 HB), whereas strontium leaves it practically unchanged (A → C: 85.7 → 86.2 HB). The hardness increase is consistent with a contribution from the hard second-phase particles introduced by the CuSn5 addition, although solid-solution effects and other composition-dependent contributions cannot be separated from it by hardness measurement alone.

This mechanism is consistent with four observations taken together. It is offered as a hypothesis, not as a demonstrated causal chain:

(i) The cutting force does not change. Particle fracture is a local event and does not appreciably alter the bulk shear strength of the material. Cutting force would be expected to be insensitive to an addition at this level — and the measured difference is indeed zero

(p = 0.94). Strontium, by contrast, converts the eutectic into a continuous fibrous structure (Fig. 1C), altering the plastic behaviour of the material at *bulk* scale and raising the cutting force.

(ii) The Ff/Fc ratio falls. Brittle fracture reduces the ploughing component; the feed force declines relative to the cutting force. The fall of the ratio from 0.550 to 0.434 in the copper–tin-bearing groups is consistent with this expectation.

(iii) Insensitivity to feed. Particle fracture produces surface damage largely independent of feed. Roughness therefore remains high even at the lowest feed in the copper–tin-bearing groups, giving rise to the two-family structure seen in Sect. 3.3.

(iv) Built-up edge increases, but conditioning on it changes little. Discrete hard particles may create local adhesion nuclei on the tool face, which would account for the increase in built-up edge measured in Sect. 4.1 (2.44 vs 1.83). If the surface damage arises principally from particle fracture, built-up edge would be a *by-product* of this chain rather than a link in it — consistent with the small attenuation observed when the built-up-edge score is entered into the model.

The chip photographs point in the same direction (Fig. 9). In groups A and C, which contain no copper–tin, the chips are long, continuous and openly helical, whereas groups B and D produce markedly short and broken chips. Easily broken chips are consistent with increased brittleness or a local loss of ductility, although chip breakability alone does not establish a change in the bulk mechanical behaviour of the material.

Fig. 9 Chip morphology in the four material groups. V = 95 m/min; in each panel, left to right, f = 0.08 · 0.16 · 0.32 mm/rev (experiments 4–6, 13–15, 22–24, 31–33). Scale is read from the rule in each photograph (cm). In groups A and C, which contain no copper–tin, the chips are long and continuously helical; in the copper–tin-bearing groups B and D they are short and broken. No image processing was applied beyond cropping of the empty background (Sect. 2.6)

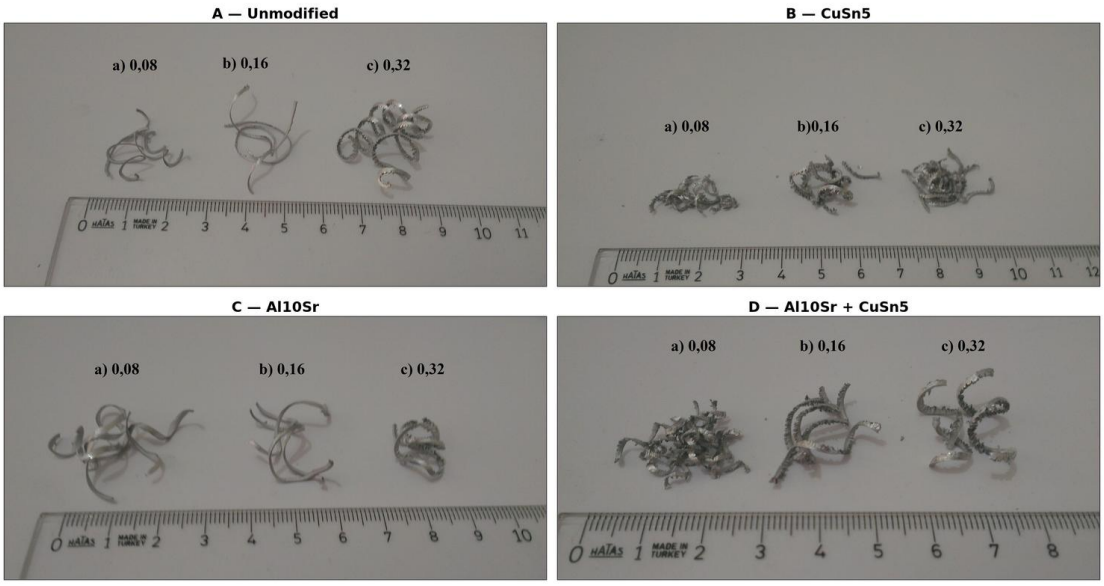


Fig. 9

It must be emphasised that this observation is **not quantitative**: chip length and ISO 3685 class were not measured, and the photographs offer a qualitative impression. The mechanism is therefore a hypothesis; its confirmation would require microstructural examination of the machined surfaces and chip roots.

The result is nonetheless practically striking. Copper and tin are conventionally described in the casting literature as elements that **improve machinability** — copper through strength and hardness, tin through chip breaking and bearing properties. In these data the copper–tin addition did indeed improve chip breakability, but **degraded surface quality by 71 %.** The phrase "improves machinability" is misleading unless the machinability criterion is specified.

4.3 Comparison with the literature

The findings agree with the literature in part and diverge from it in part. The divergences are not randomly distributed (Table 14).

Table 14 Comparison of the findings with the literature

Finding	Literature	This study	Status
Feed dominates cutting force	Established	63.6 %	✓ Agrees
Fc feed exponent ≈ 0.75–1.0	Established	0.871	✓ Agrees
Fc falls as cutting speed rises	Established	31.0 → 19.8 N	✓ Agrees
Al_2Cu forms in interdendritic	[19]	Basis of the proposed	✓ Agrees

Finding	Literature	This study	Status
regions		mechanism	
Sr raises cutting force	[15, 30] (turning)	**+44 % (p < 0.001)**	✓ Agrees
Sr **improves** surface roughness	[30] (turning); casting literature [1, 4]	**No effect (p = 0.58)**	✕ Diverges
Cu addition **improves** surface roughness	[17] (drilling)	**71 % worse (p < 0.001)**	✕✕ Opposite
Cu addition **reduces** built-up edge	[17, 26] (drilling)	**Increases it** (2.44 vs 1.83; p = 0.005)	✕✕ Opposite
Cu addition **lowers** force	[17] (drilling)	**No effect (p = 0.94)**	✕ Diverges

The findings concerning cutting mechanics agree fully with the literature. The dominance of feed, the reduction of force with cutting speed and the power-law exponents all lie in the expected ranges, which supports the physical consistency of the measurement set.

The strontium finding agrees in part. The result that strontium raises the cutting force is in the same direction as the study reporting a negative effect of strontium on machinability in the turning of an Al-Si-Cu alloy [15] and the study showing that strontium addition raises the cutting force in an Al-Mg_2Si composite [30]. The divergence is in surface roughness: [30] reports that strontium *lowers* roughness, whereas no measurable effect was found here. This is not a contradiction but a **difference in effect magnitude**; the different material system (Al-Mg_2Si versus Al-12Si) and the different Sr level may account for it.

The principal divergence concerns copper — and its direction is clearly opposite. Bayraktar and Afyon report that the Al-7Si-4Zn-3Cu alloy gave both the lowest thrust force and the lowest surface roughness, and that the most severe built-up edge was observed in the **copper-free** alloys [17]. Tash and co-workers likewise report less edge build-up in the copper-bearing 319 alloy [26]. Two of the three findings in the present data are the reverse.

The structure of this divergence does not appear accidental. **Both studies giving the opposite result are drilling studies, and both studies giving concordant results are turning studies.** There may be a physical reason. In drilling the chip is confined within the flute and must be evacuated; a brittle, easily broken chip is an advantage under these conditions and reduces build-up on the cutting edge. In turning, by contrast, the machined surface is generated directly in the region traversed by the tool nose, and the fracture of brittle particles is transferred to the surface immediately. The same microstructural change — discrete brittle particles in the interdendritic regions — may therefore be helpful in one operation and harmful in another.

This interpretation is a hypothesis and cannot be tested with the present data. Three points that weaken it must be stated explicitly:

1. **The compositions do not match.** Reference [17] contains 3 % Cu + 4 % Zn and [26] 3–4 % Cu, whereas the present alloys contain 1.05 % Cu + 0.07 % Sn. The amount of the Al_2Cu phase varies with copper content, and the independent effect of tin cannot be separated from these data.
2. **The phase morphology may not match.** Basavakumar and co-workers report that *finely and uniformly distributed* $CuAl_2$ particles give better surface characteristics [19]. The specimens in this study were not grain refined and the copper was introduced via a master alloy; the resulting Al_2Cu is plausibly coarser and less uniformly distributed. If so, the source of the divergence may be not the presence of copper but the **morphology of the phase**.
3. **The closest comparison is missing.** The direct force and roughness comparison between the two alloys in the study that turned Al-12Si and Al-12Si-3Cu [19] could not be accessed. That comparison is the most direct evidence available for distinguishing whether the divergence here originates from the operation or from the composition.

In sum, this study shows that the effect of copper on machinability is less directionally determined than the literature suggests. **The statement "copper improves machinability" cannot be used without specifying the operation and the criterion** — which is an independent confirmation of the central claim of this paper.

4.4 Practical implications

Alloy selection depends on the criterion. Where cutting force and tool load take priority, strontium modification should be avoided; where surface quality takes priority, the copper–tin addition should be avoided. The two criteria cannot be prioritised simultaneously, because within this system they respond to different additions.

Reducing the feed does not buy surface quality in CuSn5-bearing alloys — within the range investigated. As shown in Sect. 3.3, roughness is insensitive to feed in these groups. Seeking surface quality by extending cycle time is inefficient for these materials; the quality limit lies in the material. This recommendation is restricted to feeds of 0.08–0.32 mm/rev, cutting speeds of 35–135 m/min, a depth of cut of 1 mm, the tested Al-12Si composition and the particular tool–workpiece system; outside that window the response is unknown.

Single-response optimisation is misleading. As shown in Sect. 3.5, cutting force points to f = 0.08 and surface roughness to f = 0.16. Moreover, on the cutting-force criterion the "best material" changes according to whether the mean or the S/N ratio is considered.

---

5 Limitations

Sample and scope. The study rests on 36 experiments, a single base alloy, a single insert grade and a fixed depth of cut. The findings are valid within these conditions. In particular,

the behaviour of the copper–tin effect at copper contents other than 1.05 % cannot be inferred from these data, and the effect of tin cannot be separated from that of copper.

Replication. Both responses rest on a single machining run per cell, and in both cases the error term was estimated by pooling higher-order interaction terms rather than from measured pure error. The three roughness readings per run are measurement replicates and do not constitute experimental replication; the design is therefore unreplicated for both responses. This is the principal statistical limitation of the study.

The embedded 2 × 2 design. The decomposition in Sect. 2.2 was not intended in the original experimental design. It is statistically valid because the compositions are balanced, but the small differences in the Sr and Sn contents (0.156/0.153 % and 0.067/0.074 %) introduce a small uncertainty into the decomposition.

Data consistency. For eight of the cutting force values, records exist from two different processing rounds. The values published in [27] were taken as the baseline. The sensitivity analysis in Sect. 3.1.3 shows that the main findings are independent of this choice.

Experiment 36. Some of the raw records for this experiment were lost during the original study and were derived from experiment 35; the measured force and roughness values are retained as published in [27].

Run order and tool wear. The order in which the 36 runs were performed, whether that order was randomised, whether a single insert was used throughout or replaced at defined intervals, and how edge condition was controlled between runs are not recorded in the source documentation available for this re-analysis. If the runs were executed in a systematic order, progressive tool wear or thermal drift could in principle be confounded with the material and process factors, and surface roughness is the response most exposed to that risk. No flank-wear parameter was measured. The insert was imaged after each run and the built-up-edge scores show no association with cutting speed ($\rho = -0.009$) and no monotonic trend with run number, which is not consistent with strong progressive degradation, but this is indirect evidence and does not substitute for a documented run order. **Experimental run order and tool-replacement history could not be reconstructed from the source documentation; residual confounding by experimental sequence or by change in tool condition therefore cannot be completely excluded.**

Built-up-edge scoring. This analysis has four limitations, none of which should be concealed:

1. The grades used in the analysis are those of a **single assessor** (the author). The reported figures (80 % exact agreement; weighted $\kappa = 0.764$) express **agreement with an AI-assisted preliminary scoring**, not inter-observer agreement between independent human assessors, and therefore do not establish observer-independent reliability. No reliability statistic for the scale is available.
2. The preliminary grades were visible in the working file during the author's grading, so the comparison is not blinded and the agreement figure is likely to be optimistic.

3. Three of the images were recorded with the **backscattered-electron (BSE) detector**, which provides compositional rather than topographic contrast; these three images are not comparable on the same scale as the others.
4. Images for three experiments are not available as separate files.

The values in Table 13 were computed over all 36 observations. When the six problematic rows are excluded (n = 30) all results are preserved: BUE–Ra $\rho = +0.499$ ($p = 0.005$), BUE–Ff/Fc $\rho = -0.388$ ($p = 0.034$), and the attenuation test gives $F(3,23) = 24.61 \rightarrow F(3,22) = 21.47$. Nonetheless the scoring rests on a qualitative scale; profilometric quantification would have been preferable.

Chip morphology. The observation in Fig. 9 is qualitative. Chip length was not measured and no ISO 3685 classification was performed, so the chip evidence supports the mechanistic reading only descriptively and carries no inferential weight.

Quantitative microstructure. The microstructural interpretation in Sect. 2.2 is likewise qualitative. Eutectic silicon spacing, particle number density, size distribution and area fraction were not measured. Automated thresholding of the available micrographs was considered and rejected: illumination and etch response differ visibly between the four panels, so a threshold-based area fraction would be confounded with imaging conditions rather than reflecting the microstructure. Quantitative characterisation on freshly prepared sections is listed under future work.

Microstructure. The proposed mechanism has not been verified by microstructural examination of the machined surfaces or chip roots, and the identity of the second phase was not determined (no EDS or backscattered-electron imaging). The present data support the mechanism but do not prove it.

---

6 Conclusions

1. In the dry turning of modified Al-12Si alloys the two additions have **response-specific dominant effects.** Strontium raises the cutting force by 44 % ($p < 0.001$) with no detectable effect on surface roughness ($p = 0.65$). The CuSn5 addition degrades surface roughness by 71 % ($p < 0.001$) with no detectable effect on cutting force ($p = 0.94$). The two effects are not fully independent: a significant Sr × CuSn5 interaction on cutting force ($p = 0.040$) shows that the strontium effect is smaller, though still large and of the same sign, when CuSn5 is also present.

2. Bootstrap confidence intervals bound both null effects: the strontium effect on roughness is at most 29 %, and the CuSn5 effect on force at most 41 %, of the corresponding non-null effect. This rules out limited measurement sensitivity as the sole explanation, but does not establish formal equivalence.

3. Once the copper–tin variable enters the model, material group makes no further contribution to surface roughness ($F(2,29) = 0.61$; $p = 0.55$). Within the present model and experimental range, therefore, the material-group contribution to Ra is accounted for by the CuSn5 term.

4. Surface roughness is **insensitive to feed** in copper–tin-bearing alloys; reducing the feed does not gain surface quality (CuSn5 × feed interaction, 9.6 %; $p < 0.001$).

5. **Built-up edge accounts for little of the effect.** The CuSn5 addition raises built-up-edge severity ($p = 0.005$), but entering this variable into the model attenuates the CuSn5 effect on surface roughness by only 11 %. The findings are consistent with parallel effects of a **common material-related cause**, offered as a candidate mechanism rather than a demonstrated one. No effect of strontium on built-up edge was detected, but the resolution of the scale was insufficient to bound that null.

6. **A candidate common cause is visible in the microstructure:** the CuSn5-bearing groups contain discrete, angular second-phase particles absent in the others. The identity of the phase could not be determined at optical magnification and no EDS was performed, so the mechanism remains a hypothesis. Copper and tin were introduced together and cannot be separated in this design.

7. The force-component ratio **Ff/Fc** retains a significant inverse association with surface roughness after cutting speed, feed, material and cutting force are all controlled ($F(1,29) = 4.99$; $p = 0.033$), whereas cutting force adds nothing once material is in the model ($p = 0.53$).

8. **Cross-validation is essential in small samples.** For cutting force the model with the highest R^2 (0.903) does not give the lowest prediction error. For surface roughness the decisive element is not model order but a single **CuSn5 × feed** interaction term, which lowers the LOOCV error from 0.68 to 0.50 μm.

9. **Flexible learners offer no predictive advantage at this scale.** For cutting force, the regression tree, random forest and k-nearest neighbours all fall behind the five-parameter linear model. For surface roughness the tree outperforms the linear model, but its advantage disappears once the same interaction term is written explicitly into the parametric model (0.50 versus 0.49). At this scale of design, flexible learners are useful as tools of discovery, not of prediction.

10. **Machinability cannot be summarised by a single criterion.** Within the same dataset, the force criterion and the surface criterion point to different alloying elements, different feed levels and different "best materials".

Future work. Determination of the identity of the discrete second phase by EDS or backscattered-electron imaging; quantitative microstructural characterisation (eutectic spacing, particle size distribution and area fraction) on freshly prepared sections; an experiment in which copper and tin are varied independently, since the present design cannot separate them; microstructural examination of machined surfaces and chip roots; quantification of built-up edge with inter-observer agreement or by profilometry; a dose–response design in which copper content is varied systematically; and turning and drilling the same alloys in order to test the operation dependence of the copper effect.

References

1. Kaufman JG, Rooy EL (2005) Aluminum alloy castings: properties, processes, and applications. ASM International / American Foundry Society, Materials Park, OH

2. Dahle AK, Nogita K, McDonald SD, Dinnis C, Lu L (2005) Eutectic modification and microstructure development in Al–Si alloys. Mater Sci Eng A 413-414:243-248. https://doi.org/10.1016/j.msea.2005.09.055

3. Faraji M, Katgerman L (2009) Microstructural analysis of modification and grain refinement in a hypoeutectic Al–Si alloy. Int J Cast Met Res 22:108-110. https://doi.org/10.1179/136404609X367461

4. Gruzleski JE, Closset BM (1990) The treatment of liquid aluminum-silicon alloys. American Foundrymen's Society, Des Plaines, IL

5. Nogita K, McDonald SD, Dahle AK (2004) Eutectic modification of Al-Si alloys with rare earth metals. Mater Trans 45:323-326. https://doi.org/10.2320/matertrans.45.323

6. Faraji M, Todd I, Jones H (2009) Effect of phosphorus and strontium additions on formation temperature and nucleation density of primary silicon in Al–19 wt.% Si alloy. Metall Mater Trans A 40:1710-1715. https://doi.org/10.1007/s11661-009-9842-0

7. Farahany S, Idris MH, Ourdjini A, Faris F, Ghandvar H (2015) Evaluation of the effect of grain refiners on the solidification characteristics of an Sr-modified ADC12 die-casting alloy by cooling curve thermal analysis. J Therm Anal Calorim 119:1593-1601. https://doi.org/10.1007/s10973-014-4367-1

8. Farahany S, Ourdjini A, Idris MH, Shabestari SG (2013) Evaluation of the effect of Bi, Sb, Sr and cooling condition on eutectic phases in an Al–Si–Cu alloy (ADC12) by in-situ thermal analysis. Thermochim Acta 559:59-68. https://doi.org/10.1016/j.tca.2013.02.024

9. Totten GE, MacKenzie DS (2003) Handbook of aluminum, volume 1: physical metallurgy and processes. Marcel Dekker, New York

10. Geçgel B, Altıntaş Y, Arslan M, Çelen O, Kocaman E, Koçar O (2023) Effect of silicon on machinability in AlSi6, AlSi12 and AlSi18 alloys. Silicon 16:1467-1479. https://doi.org/10.1007/s12633-023-02760-5

11. Akyüz B (2016) Effect of silicon content on machinability of Al-Si alloys. Adv Sci Technol Res J 10:51-57. https://doi.org/10.12913/22998624/64153

12. Wada T (2015) Si particle size-controlled Al-17 mass% Si alloy and tool wear in cutting Al-17 mass% Si alloy by polycrystalline diamond tool. Appl Mech Mater 798:372-376. https://doi.org/10.4028/www.scientific.net/AMM.798.372

13. Roy P, Sarangi SK, Ghosh A, Chattopadhyay AK (2009) Machinability study of pure aluminium and Al–12% Si alloys against uncoated and coated carbide inserts. Int J Refract Met Hard Mater 27:535-544. https://doi.org/10.1016/j.ijrmhm.2008.04.008

14. Chattopadhyay AK, Roy P, Ghosh A, Sarangi SK (2009) Wettability and machinability study of pure aluminium towards uncoated and coated carbide cutting tool inserts. Surf Coat Technol 203:941-951. https://doi.org/10.1016/j.surfcoat.2008.08.047

15. Barzani MM, Farahany S, Yusof NM, Ourdjini A (2013) The influence of bismuth, antimony, and strontium on microstructure, thermal, and machinability of aluminum-silicon alloy. Mater Manuf Process 28:1184-1190. https://doi.org/10.1080/10426914.2013.792425

16. Barzani MM, Sarhan AAD, Farahany S, Ramesh S, Maher I (2015) Investigating the machinability of Al–Si–Cu cast alloy containing bismuth and antimony using coated carbide insert. Measurement 62:170-178. https://doi.org/10.1016/j.measurement.2014.10.030

17. Bayraktar Ş, Afyon F (2020) Machinability properties of Al–7Si, Al–7Si–4Zn and Al–7Si–4Zn–3Cu alloys. J Braz Soc Mech Sci Eng 42:116. https://doi.org/10.1007/s40430-020-02281-x

18. Marani Barzani M, Zalnezhad E, Sarhan AAD, Farahany S, Ramesh S (2015) Fuzzy logic based model for predicting surface roughness of machined Al–Si–Cu–Fe die casting alloy using different additives-turning. Measurement 61:150-161. https://doi.org/10.1016/j.measurement.2014.10.003

19. Basavakumar KG, Mukunda PG, Chakraborty M (2007) Influence of melt treatments and turning inserts on cutting force and surface integrity in turning of Al–12Si and Al–12Si–3Cu cast alloys. Surf Coat Technol 201:4757-4766. https://doi.org/10.1016/j.surfcoat.2006.10.015

20. Grum J, Kisin M (2003) Influence of microstructure on surface integrity in turning — part I: the influence of the size of the soft phase in a microstructure on surface-roughness formation. Int J Mach Tools Manuf 43:1535-1543. https://doi.org/10.1016/S0890-6955(03)00199-8

21. Grum J, Kisin M (2003) Influence of microstructure on surface integrity in turning — part II: the influence of a microstructure of the workpiece material on cutting forces. Int J Mach Tools Manuf 43:1545-1551. https://doi.org/10.1016/S0890-6955(03)00200-1

22. Davim JP, Baptista AM (2000) Relationship between cutting force and PCD cutting tool wear in machining silicon carbide reinforced aluminium. J Mater Process Technol 103:417-423. https://doi.org/10.1016/S0924-0136(00)00495-7

23. Kılıçkap E, Çakır O, Aksoy M, İnan A (2005) Study of tool wear and surface roughness in machining of homogenised SiC-p reinforced aluminium metal matrix

composite. J Mater Process Technol 164-165:862-867. https://doi.org/10.1016/j.jmatprotec.2005.02.109

24. Pul M (2019) Investigation of cutting tool wear behaviors in machining of silicon carbide and magnesium oxide reinforced aluminium composites. Mater Res Express 6:1065d1. https://doi.org/10.1088/2053-1591/ab4093

25. Bao H, Stevenson MG (1976) An investigation of built-up edge formation in the machining of aluminium. Int J Mach Tool Des Res 16:165-178. https://doi.org/10.1016/0020-7357(76)90002-0

26. Tash M, Samuel FH, Mucciardi F, Doty HW, Valtierra S (2006) Effect of metallurgical parameters on the machinability of heat-treated 356 and 319 aluminum alloys. Mater Sci Eng A 434:207-217. https://doi.org/10.1016/j.msea.2006.06.129

27. Keser M (2015) Effect of the modification process on the machinability of cast Al12Si alloy. MSc thesis, Sakarya University, Graduate School of Natural and Applied Sciences, Sakarya, Türkiye. Turkish Council of Higher Education Thesis Centre, no. 413296

28. ISO 3685:1993 Tool-life testing with single-point turning tools. International Organization for Standardization, Geneva

29. ISO 4288:1996 Geometrical product specifications (GPS) — surface texture: profile method — rules and procedures for the assessment of surface texture. International Organization for Standardization, Geneva

30. Razavykia A, Farahany S, Yusof NM (2015) Evaluation of cutting force and surface roughness in the dry turning of Al–Mg2Si in-situ metal matrix composite inoculated with bismuth, antimony and strontium. Measurement 76:170-182. https://doi.org/10.1016/j.measurement.2015.08.032

Statements and Declarations

Funding. This research received no specific grant from any funding agency in the public, commercial or not-for-profit sectors.

Competing interests. The author declares no competing interests.

Ethics approval. Not applicable. This study does not involve human participants or animals.

Data and reproducibility. All analyses and Figs. 2–7 are generated from a 36-row raw data file by scripts. **No external statistical or machine-learning library was used at any stage** — including the analysis of variance, regression, cross-validation and the three flexible learners of Sect. 3.7; all procedures were coded explicitly. The dataset and all analyses are collected in a single Jupyter notebook that reproduces every number in the

paper from scratch; the data are embedded in the notebook, so no external file is required. The notebook is submitted as Online Resource 1 and contains the complete 36-run dataset, so no separate data file or repository deposit is needed to reproduce the results.

Image integrity. The photographs in Figs. 1, 8 and 9 are original records. The only operations applied were the masking of the institution name and instrument brand in the SEM images and the cropping of empty background in the chip photographs. Scale bars and SEM measurement information were preserved. See Sect. 2.6.

AI use statement. A large language model (Anthropic Claude) was used as an assistant in preparing the analysis code, the figure-generating scripts, the manuscript text, the literature search and a preliminary set of built-up-edge grades. Full details are given in Sect. 2.5. All numerical results were regenerated and verified by the author against the raw data; every bibliographic entry was verified against Crossref; the built-up-edge grades used in the analysis are the author's own. The author takes full responsibility for the accuracy and integrity of the work. The AI tool does not meet authorship criteria and is not listed as an author.

Author contributions. The manuscript has a single author, who is responsible for the conception, analysis, figure preparation and writing of the work.

Supplementary Files

This is a list of supplementary files associated with this preprint. Click to download.

- OnlineResource1.zip